This is the peer-reviewed, final accepted version for American Mineralogist, published by the Mineralogical Society of America.
The published version is subject to change. Cite as Authors (Year) Title. American Mineralogist, in press.
DOI: https://doi.org/10.2138/am-2021-7783. http://www.minsocam.org/

Revision 1

Re-examined heterotype solid solution between calcite and strontianite and Ca-Sr fluid-carbonate distribution: an experimental study in the system $CaCO_3$–$SrCO_3$–H_2O at 0.5–5 kbar and 600°C

Ferry Schiperski[*,1], Axel Liebscher[2], Matthias Gottschalk[3], Gerhard Franz[1]

[1] Technische Universität Berlin, Dept. of Applied Geosciences, Applied Geochemistry, 10587 Berlin, Germany

[2] Helmholtz Centre Potsdam, GFZ German Research Centre for Geosciences, Telegrafenberg, 14473 Potsdam, Germany
now: Federal Office for the Safety of Nuclear Waste Management, 10623 Berlin, Germany

[3] Helmholtz Centre Potsdam, GFZ German Research Centre for Geosciences, Telegrafenberg, 14473 Potsdam, Germany

[4] Technische Universität Berlin, Dept. of Applied Geosciences, Applied Geochemistry, 10587 Berlin, Germany

*** corresponding author at: Ernst-Reuter-Platz 1, 10587 Berlin, Germany.**

Tel.:+493031472652; E-mail address: schiperski@tu-berlin.de (F. Schiperski)

Key words: strontianite, Sr-calcite, Sr-aragonite, carbonate solid solution, Sr-cycle

Abstract

Carbonates are excellent carriers for bivalent cations such as Ca, Mg, and Sr, and their stability and solid solution is important for the global Sr-cycle. To shed light on the topology of the two-phase field between calcite-type and aragonite-type (Ca, Sr)CO_3 solid solutions as function of P and T, and on the distribution of Sr and Ca between carbonates and fluid, we performed an experimental study in the system $CaCO_3$–$SrCO_3$–H_2O; run conditions were 600°C and 0.5 kbar to 5 kbar. Conventional and rapid quench hydrothermal synthesis techniques and different starting materials were used, all with bulk compositions being within the assumed/postulated two-phase field of calcite-type and aragonite-type (Ca, Sr)CO_3 solid solutions. Run products were analyzed by scanning electron microscopy, electron microprobe analysis, and powder X-ray diffraction with Rietveld refinement. The results show that the heterotype solid solution is larger than previously assumed: calcite incorporates up to 20 mol% $SrCO_3$, which is twice as much as was

predicted. Compositional range of the aragonite-type solid solution was identical to literature data. Based on the collected data an updated version of the phase diagram P-x (Sr) at 600°C for the system $CaCO_3$–$SrCO_3$ was calculated. The phase diagram does not support a phase transition within the trigonal (Ca, Sr)CO_3 solid solution related to rotational disorder of CO_3-groups. This order-disorder phase transition was previously postulated to explain some observed compositional trends in this system. Our new data are line with other recent studies. The distribution of Sr and Ca between fluid and solid $K_d = X_{Sr}^{solid}/X_{Sr}^{fluid}$ —in contrast to silicate-fluid systems that typically show clear preference of Sr over Ca for the fluid phase—is near to 1.0 for calcite-type and on the average around 2.0 for aragonite-type solid solutions.

Introduction

Due to the same ionic charge and a comparable ionic radius Ca and Sr are interchangeable to a certain extent in carbonates with trigonal (Cal-type) and orthorhombic (Arg-type) structure at subsolidus conditions (Chang 1965, 1971; Froese and Winkler 1966; Carlson 1980). Striking feature of the stability relations in the system (Sr, Ca)CO_3 is the occurrence of a two phase field of coexisting Cal-type and Arg-type (Sr, Ca)CO_3 solid solutions (Fig. 1A and B). At atmospheric pressure and a temperature of 600°C the extent of this field is about 30 mol% and narrows with increasing pressure towards the phase transition Cal/Arg (Fig. 1B). The occurrence of a trigonal disordered phase (rotational disorder of CO_3-groups; Fig. 1A and B) was postulated by Carlson (1980) based on own experiments and data from Goldsmith and Newton (1969; See Fig. 1C), although the latter data were already questioned at that time (e.g. Mirwald 1976). The stability and extent of (Ca,Sr)-solid solutions and the solid fluid-distribution of Ca and Sr are of general importance for the global Sr-cycle (e.g. Kump 1989). Besides the carbonates studied here, other

minerals relevant to the Sr-cycle are anorthite, lawsonite, slawsonite, walstromite, zoisite, grossularite, and margarite (Dörsam et al. 2007; Liebscher et al. 2009, 2010).

No compositional data from experimental studies on $(Ca,Sr)CO_3$ solid solutions at elevated pressure and temperature exist that are based on electron microprobe analyses (EMPA) or comparable spatially resolving analytical methods. Previous studies relied on powder X-ray diffraction (XRD) with calibration curves for $X_{Sr} = Sr/(Sr+Ca)$ versus peak position (e.g. Froese and Winkler 1966; Chang 1965) or appearance/disappearance method (Carlson, 1980) which are prone to error in cases of strongly zoned run products as are often observed in synthesis experiments involving solvent-mediated phase transformation or kinetically sluggish mineral systems, respectively (e.g. Fernández-González 1999; Putnis 2009).

This study experimentally re-examines the subsolidus phase relations of the heterotype solid solutions of Cal-type and Arg-type Ca-Sr carbonates at 600°C and 0.5–5 kbar using different experimental approaches and starting materials. State-of-the-art analyses (XRD with Rietveld refinement, EMPA, scanning electron microscopy SEM, inductively-coupled optical emission spectroscopy ICP-OES) provide necessary chemical and structural resolution to construct a revised two-phase field that is verified by thermodynamic modelling. The experimental data also allow to determine the distribution of Ca and Sr between carbonates and hydrous fluids.

Experimental Approach

Three types of starting materials were prepared (Table 1) with initial bulk X_{Sr} within the assumed two-phase field of Cal-type and Arg-type solid solutions based on previous studies (Fig. 1B). These compositions were treated hydrothermally assuming reactions towards the stable compositions. Experiments of type I started from pure strontianite, calcite, and deionized water; experiments of type II from synthetic pure strontianite, natural aragonite with $X_{Sr}<0.005$, and

This is the peer-reviewed, final accepted version for American Mineralogist, published by the Mineralogical Society of America.
The published version is subject to change. Cite as Authors (Year) Title. American Mineralogist, in press.
DOI: https://doi.org/10.2138/am-2021-7783. http://www.minsocam.org/

deionized water; experiments of type III started from metastable Sr-bearing aragonite (with X_{Sr} = 0.24 and 0.37) synthesized following the procedure proposed by Wang et al. (1999).

Solid run products were examined by SEM and partly embedded in epoxy resin, ground and polished for EMPA. Fluids were extracted after runs and analyzed for Ca and Sr. This procedure has the disadvantage that it does not necessarily represent the equilibrium due to potential quench products. However, insoluble quench products are less likely in the simple system Ca-Sr-CO_2 and our approach is considered sufficient to estimate the Ca-Sr distribution between fluid and the two types of carbonates.

Material and Methods

Experimental Methods

Experiments are listed in Table 1. Experiments of type I ('Cal+Str') were prepared from synthetic strontianite (Sigma-Aldrich, 204455-5G, 99.995% purity), synthetic calcite (Sigma-Aldrich, 202932-5G, 99.995% purity), and deionized water. Experiments of type II ('Arg+Str') were prepared from synthetic pure strontianite, natural aragonite with X_{Sr}<0.005 (mineralogical collection TU Berlin, Minglanilla locality, Spain), and deionized water. For experiments of type III ('Sr-Arg') two metastable Sr-aragonite compositions with X_{Sr} = 0.24 and 0.37, respectively, were synthesized following the procedure proposed by Wang et al. (1999) and adding defined amounts of Sr (Table S1). Phase purity of the starting materials in all synthesis types was verified by XRD analyses and chemical composition by scanning electron microscopy accompanied by energy dispersive X-Ray analyses (SEM-EDX).

Starting materials were ground and homogenized in an agate mortar after being dried for 3 h at 150°C. 50–150 mg of solids and 10–20 ml deionized water were loaded in gold or platinum

capsules (3 mm×30–40 mm), pre-cleaned in 36-%-hydrochloric acid for at least one hour at 70°C and rinsed with deionized water and acetone. After loading, the capsules were welded shut and checked for weight loss after being heated to 150°C for 12 hours.

Experiments were conducted at 0.5 kbar to 5 kbar and at 600°C for 3 to 22 days except for P6 that was run at 550°C (Table 1). Two types of hydrothermal systems were used, a conventional system at the Technische Universität Berlin, and a rapid quench system at the German Research Center for Geosciences (GFZ) Potsdam. Peak temperature was reached within one hour and was measured using NiCr-Ni thermocouples with an estimated error of < ±10°C. Water served as pressure medium and pressure was measured with a calibrated strain gauge with an estimated error of < ±0.1kbar. Samples were quenched to room temperature within 3 to 5 min and within few seconds using the conventional and the rapid-quench setup, respectively. After weighting to check for leakage, the capsules were pierced and rinsed under deionized water in a beaker for avoiding any loss of fluid, which was successfully done in previous studies (e.g. Liebscher et al. 2009). All of the material was filtered through a pre-cleaned and dried zeolite filter with a nominal pore size of 2 µm. After the water of the beaker was emptied, the solids were further rinsed with deionized water until 50 ml or 100 ml of water were collected, respectively. The fluid was stored air-tight in PET bottles, the solids were dried overnight at 100°C.

Analytical Methods

XRD. Powder XRD was performed on a PW 1050 (Philips) with a Cu anode operating at 40 kV and 40 mA, equipped with a primary Ni-monochromator. Data were collected between 5 and 80° 2θ in reflection mode with a step width of 0.02° 2θ and an integration time of 10 s. Phase identification was performed using X'Pert Highscore (Version 1.0, Philips) and Rietveld refinement was done to yield lattice parameters and phase fractions using GSAS I (Larson and

Von Dreele, 1994). Estimated errors are low with 6σ mainly ranging in the third to forth decimal digit for all lattice parameters (Table S2). Structural data for initial phase parameters of the refinement were taken from the Inorganic Crystal Structure Database (ICSD) for strontianite (Jarosch and Heger 1988) and calcite (Markgraf and Reeder 1985).

SEM. Secondary electron images, backscattered electron images, and energy dispersive X-ray spectra were recorded on a S-520 scanning electron microscope (Hitachi) at the Central Facility for Electron Microscopy at the TU Berlin (ZELMI). Samples were loaded on adhesive carbon strips and coated with carbon. EDX spectra were recorded at 500 nA and 20 kV at integration times of 100 s and 200 s.

EMPA. Run products were embedded in epoxy resin, ground and polished. Wavelength-dispersive X-ray spectroscopy (WDX) was performed using a JEOL Hyperprobe JXA-8530F equipped with a thermal field emission gun and 5 spectrometers at ZELMI. Probe current was set to 5 nA at 15 kV alteration voltage. Counting time on peaks and background was 20 s and 10 s, respectively. Natural calcite (Ca, Iceland Spar, Jarosewich and MacIntyre 1983) and natural strontianite (Sr, Smithonian Standard, Jarosewich and White, 1987) were used as standards. Data correction was automatically performed using the PRZ-algorithm (Armstrong, 1995). A beam diameter of 1 µm was chosen, resulting in a penetration depth of 3 µm based on Monte Carlo simulation for strontianite. Oxide masses of Ca and Sr were converted into $CaCO_3$ and $SrCO_3$ assuming stoichiometric amount of CO_2 giving mean totals of 99.5 wt% with minima and maxima of 94.6 and 105.5 wt%, respectively.

Fluids. Fluids were analyzed for Ca and Sr by inductively-couplled optical emission spectroscopy (ICP-OES) with an instrument of the company VARIAN type ICP-OES VISTA MPX (GFZ Potsdam). Calcium was determined on the 422.673 nm line, Sr on the 407.771 nm

line. The result generally presents the arithmetic mean of minimum three measurements in diluted fluids 1:9, standard deviation refers to all measurements.

Results and Discussion

Phase identification and lattice parameters

Both Arg-type and Cal-type carbonates were identified in all experiments. Phase proportions and composition, however, differ between runs and types of starting material (Fig. 2). Only synthesis of type III showed a two phase field in which Cal-type and Arg-type $(Sr,Ca)CO_3$ solid solutions coexist over the whole range of pressure. In all type III experiments, newly formed Arg-type and Cal-type $(Ca,Sr)CO_3$ solid solutions were identified. No intermediate (metastable) Arg-type solid solution remained but new Sr-calcite and Ca-strontianite or Sr-aragonite formed. Most synthesises of type I and II lacked either Sr-incorporation into calcite or Ca-incorporation into aragonite or both, and some of the starting materials remained unaffected in this type of synthesis.

Structural parameters were determined for the main phases that are expected to represent equilibrium conditions based on the absence or only marginal quantities of starting materials or intermediate phases for most of the runs. Strontium content and lattice parameters *a*, *b*, and *c* of Arg-type solid solutions are well correlated and in trend with experimental data from Holland et al. (1963) and Lucas-Girot et al. (2007) who also observed a linear trend for X_{Sr} from 0 to 0.4, 0.7 to 1.0, and 0 to 0.5 (Fig. 3), and with computational studies (Dudnikova et al. 2015). Linear correlation of a combined data set including data of other studies (Holland et al. 1963; Lucas-Girot et al. 2007; Antao and Hassan 2009) is excellent ($r^2 = 0.994$ to 0.997) and proof a linear trend of all parameters within the range of uncertainties (Fig. 3).

Lattice parameters *a* and *c* of the Cal-type phase increase with increasing Sr content. A trend is less obvious compared to the Arg-type phase since only a small range of composition is covered. Also, data scatter considerably and various points deviate significantly form a linear trend. Assuming a linear correlation, data on lattice parameters of the Cal-type phase with Sr-contents of up to 75 mol% (Fubini et al. 1988) combined with our data and data of Antao and Hassan (2009) for $X_{Sr} = 0$, yield extrapolated lattice parameters of trigonal pure $SrCO_3$ of $a = 5.08 \pm 0.02$ Å and $c = 17.62 \pm 0.10$ Å. Errors are estimated based on the extrapolation of maximum and minimum slopes within the upper and lower confidence levels towards the Sr-endmember using a 95% confidence band (Fig. 3).

Chemical composition and attainment of Equilibrium

Type I experiments. Cal-type and Arg-type phases were distinguished by their morphology in SE images and in cross sections in BSE images (Fig. 4). he Cal-type phase did not incorporate Sr as was already indicated by XRD data. Newly formed Ca-Str shows average Sr-contents between 53 to 74 mol% (Table 2). Variability of mean Sr-contents is high in individual runs and there is no correlation of X_{Sr} in Arg-type solid solutions with pressure. Arg-type crystals are zoned, mostly with Ca-free cores and elevated Ca concentrations in their fringes, both distinctly separated (Fig. 4B). This textural observation is reflected by a high standard deviation between ~11 mol% and ~46 mol% of $SrCO_3$. The shape of the Arg-type phase is irregular and often consists of grain aggregates. (Fig. 4A).

We distinguish newly formed calcite crystals from relict calcite by their shape. Newly formed calcite crystals are about 20 µm large, have an isometric-rhombohedral shape in cross section, and low Sr-contents, whereas many small, elongated rhombohedral calcite crystals are similar in

184 shape to the staring material (Fig. 4A and B). The presence of relict starting material and the
185 newly precipitated almost pure calcite crystals prove that overall equilibrium referring to the two-
186 phase field was not achieved (Fig. 1). Initial X_{Sr} of the bulk composition might have been too
187 high to trigger the precipitation of a new Ca-enriched orthorhombic phase for runs were pure
188 strontianite was formed.

189 Several approaches were made to increase the reactivity of phases within type I experiments,
190 when we realized that reactions in the first runs were incomplete. Reaction time was stepwise
191 increased from 3 to 21 days without any significant change e.g. short-time runs P2 and P3 yielded
192 similar results as long time runs P7 and P8. Silveroxalate (AgOx) was added in runs P11 and P12
193 to increase the amount of CO_2 in the fluid, which was unsuccessful as well. Potential re-
194 equilibration during quenching could be excluded by performing rapid quench experiments (P6
195 and P8).

196 **Type II experiments.** Below a pressure of 3 kbar calcite shows elevated Sr contents (Table 2).
197 These small Sr-calcite crystals (10–20 μm) form isometric, homogeneous aggregates (Fig. 4C,
198 D). At higher pressures calcite crystals are larger, partly with rhombohedral habitus, but with
199 small amounts of Sr only (Fig. 4E, F; Table 2), similar to observations in type I experiments.
200 However, for these runs elevated Sr-values can still be observed along cracks and on fringes of
201 otherwise pure calcite crystals.

202 Neither pure strontianite nor remaining aragonite from the starting material was found, which is
203 attributed to higher dissolution rates of the orthorhombic phases compared to calcite used in
204 type I experiments. The compositional range of the newly formed Arg-type solid solutions is
205 smaller compared to runs of type I (standard deviation ranges from 0.9 to 16 mol%), and
206 Sr-contents are generally lower. Crystals form aggregates similar to the Cal-type crystals.

Although Arg-type solid solutions are mostly homogenous, in some crystals a tendency of elevated Sr-contents towards the core of the crystals was observed, which points to a decreasing X_{Sr} in the fluid during the experiment. Sr-contents in Arg-type solid solutions decrease with increasing pressure (Table 2).

The small compositional zoning of the Cal-type crystals at 3 to 5 kbar pressure (P14–P16) indicates incomplete reaction of the crystals towards their presumed equilibrium composition. At 1 to 2 kbar (P9 and P10), high compositional variance due to compositional zoning of the crystals indicates disequilibrium. Only at 0.5 kbar (P13) Cal-type crystals are homogenous. This is likely explained by (1) a fluid composition during crystal precipitation that is closer to the equilibrium fluid composition compared to runs at higher pressure, (2) sufficient oversaturation of calcite-type solid solution in the fluid, and (3) fluid homogenization that is faster than the rate of precipitation.

Type III experiments. No intermediate (metastable) Arg-type solid solutions remained but new Cal-type and Arg-type phases formed. Both Cal-type and Arg-type phases incorporate high amounts of Sr and Ca, respectively. The Cal-type solid solutions have a Sr-rich core and a porous Ca-rich rim with a sharp boundary between core and rim (Fig. 4H). The outline of this porous structure mimics the original rhombohedral shape of Cal-type crystals (Fig. 4G).This zoning results in apparently lower X_{Sr} of the Cal-type solid solution based on XRD determination and emphasizes the significance of the spatially resolved microbeam analyis applied here. Entrapment of orthorhombic crystals in Sr-rich calcite cores indicate that growth of the Cal-type phase occurred after or simultaneously with the Arg-type phase. Hence, the porous rims seem to be a secondary product. Based on its habitus, it is not in equilibrium with the other precipitates.

Decomposition of Cal-type solid solutions during quenching has been observed by others (Chang 1965; Froese and Winkler 1966; Carlson 1980) and agrees with P-T-X_{Sr} relations; Sr-Cal decomposes at decreasing temperatures and becomes enriched in Ca (Fig. 1A). If quenching, however, would have produced these rims they should be present in all synthesis that produced Sr-Cal-type crystals. However, such rims were not observed in type II experiments (P10, P13) and they can therefore not be a result of quenching. A possible explanation of these fringes is that they are a result of solvent-mediated phase transformation (Putnis 2009) during the experiment, a process, in which the interface of a solid in contact with a fluid dissolves and supersaturates that fluid locally with respect to a new solid phase that immediately precipitates (Putnis 2002; Putnis and Putnis 2007). Driving factors for this process are (1) a lower molar volume of the new phase compared to the parent phase, and (2) a lower solubility of the new phase, which manifest themselves in a porosity of the new crystals (Putnis 2009). Molar volume of calcite is lower than that of its Sr-bearing endmember (Fig. 5). Crystallographic information is transferred to the new phase, which is visible in this study by pseudomorphic conservation of rhomboidal shapes (Fig. 4G, H). Porosity of the less dense Ca-rich phase allows for fluid transport and ongoing dissolution/precipitation.

The dissolving core of the crystals is therefore assumed to represent overall equilibrium conditions while Ca-enriched calcite rims represent only local re-equilibration. This will finally raise X_{Sr} in the fluid to a certain extent (see "Fluid composition").

Revised phase diagram and Ca-Sr distribution

Altogether nine runs have been identified as near-equilibrium runs, most of them resulting from type III experiments (Table 3). The P–X_{Sr} relation at 600°C based on a symmetric regular solution model was calculated using thermodynamic data mainly from Gottschalk (1997) and

252 references therein (Fig. 5; Supplement Table S3). Equilibrium equations were solved for
253 interaction parameters W_{Arg} (interaction parameter of Arg_{ss}), W_{Cal} (interaction parameter of
254 Cal_{ss}), and $\mu_{Sr\text{-}Cal}$ (chemical potential of trigonal $SrCO_3$) by least-square refinement using a
255 nonlinear solution algorithm programed in Mathematica (Version 12.0, Wolfram Research, Inc.).
256 Molar volume of 39.7 cm^3 mol^{-1} for the trigonal Sr endmember was calculated from XRD
257 measurements of this study. This value is in good agreement with extrapolating the molar volume
258 versus ionic radii of other carbonates (Ni, Mg, Zn, Co, Fe, Mn, Cd, and Ca) towards $SrCO_3$,
259 which yields 39.3 cm^3mol^{-1}. Thermal expansion and compressibility are unknown for this phase
260 and are therefore assumed to be identical to values of calcite.

261 The fitting yielded interaction parameters of $W_{Arg} = 4005 \pm 976$ kJ mol^{-1} and
262 $W_{Cal} = 5642 \pm 3526$ kJ mol^{-1}. The chemical potential of the trigonal Sr-endmember at 600°C and
263 0.1 MPa was $\mu = -1.35 \times 106 \pm 0.02 \times 106$ kJ mol^{-1}. Based on this result a forward model was
264 calculated at 600°C covering the pressure range from 0 to 15 kbar (Fig. 5).

265 **Aragonite-type solid solution.** Compositional data of the Arg-type phase are in very good
266 agreement with data from literature at 600°C (Fig. 5; Chang 1965; Chang 1971; Carlson 1980)
267 and the shape of the orthorhombic limb of the two-phase field generally agrees with studies at
268 other temperatures (e.g. Froese and Winkler 1966). Mean Sr-contents as determined in this study
269 differ by less than 2 mol% from the data of Carlson (1980) over the whole pressure range of 1 to
270 5 kbar. The thermodynamic model predicts values of about 55 mol% Sr at atmospheric conditions
271 which is identical to data obtained by Chang (1965). Data by Chang (1971) at 10 kbar deviate
272 significantly from our predictions and only strong curvature of the phase boundary line would
273 explain such behavior as was already stated by Carlson (1980). Extrapolation of experimental
274 data of this study towards pure $CaCO_3$ lies on an almost straight line and agrees with data by

Carlson (1980). In contrast, the thermodynamic model shows a slight curvature. The thermodynamic model hence slightly underestimates Sr-content below a pressure of about 1.5 kbar and slightly overestimates it at pressures above about 1.5 kbar compared to experimental data.

Calcite-type solid solution. To date, comprehensive data on the Sr-content of Cal-type solid solutions related to pressure at elevated temperatures have only been presented by Carlson (1980) and to a smaller extent by Chang (1965, 1971). Maximum Sr-content in Cal-type solid solutions of the here presented data at low pressures is only slightly higher compared to studies by Chang (1965). Data from Carlson (1980) on the Cal-type solid solution shows significantly lower Sr-values than results of this study. A major feature in Carlson´s data (1980) is a stability field of a disordered trigonal Sr-bearing calcite (rotational disorder of CO_3-groups), which was postulated to explaining a rapid increase of Sr in calcite from 3 to 4 kbar, whereas the Sr-content in calcite of the here presented experimental data is decreasing progressively with increasing pressure (Fig. 5). The phase transition between an ordered and disordered Sr-Cal was postulated by Carlson (1980) based on the existence of the phase transition at the triple point Arg–Cal I–Cal II (Fig. 1) which was used to explain the non-linearity in the phase transition Cal–Arg (Jamieson 1957; Goldsmith and Newton 1969). However, this transition could not be verified or was rejected even before 1980 (Kondo et al. 1972; Cohen and Klement 1973, Mirwald 1976; Redfern et al. 1989; Bagdassarov et al. 2003). Instead, the curvature in Cal–Arg phase transition is explained and is generally accepted to originate from a continuously increasing orientational disordering of planar CO_3^{2-} groups with increasing temperature (Redfern et al. 1989, Dove and Powell 1989; Antao et al. 2009).

Fluid composition. Determination of Ca and Sr in the fluids after run yielded values of X_{Sr}^{fluid} = Sr /Ca (molar) between 0.17 and 0.24 (Table 3). Plotting these values against X_{Sr} in the Cal-type and Arg-type solid solutions shows (Fig. 6A) that for carbonates the $K_d = X_{Sr}^{carbonate}/X_{Sr}^{fluid}$ is 0.8–1.2 for the Cal-type solid solution (comparable to data in Katz et al. 1972) and 1.7–3.1 for the Arg-type solid solution. Considering the potential shift of X_{Sr}^{fluid} towards higher values due to the solvent-mediated phase transformation (type III experiments only) towards the Ca-enriched Cal-type phase, actual X_{Sr}^{fluid} would be even lower. This is also indicated by comparing K_d from experiments at 1 kbar (type II, P10) and (type III, P22) that should bracket the "true" K_d-value. Similarity of these K_d-values (1.1 and 1.0 for the Cal-type solid solution; 2.7 and 2.2 for the Arg-type in type II and type III experiments, respectively; Table 3) also reveals that the solvent-mediated phase transformation might not significantly bias the experimental outcome of this study.

The overall results are in marked contrast to the distribution of Ca-Sr between silicates and fluid. Previous determinations for the solid-fluid distribution on anorthite, lawsonite, slawsonite, walstromite, zoisite, grossularite, and margarite (Dörsam et al. 2007; Liebscher et al. 2009, 2010) showed that in silicate-systems the fluid is always enriched in Sr compared to Ca. However, even in the here-studied carbonate system the data indicate decreasing K_d-values with increasing pressure (Fig. 4B). Data at 2 kbar are not in line with this general trend and K_d-values are generally higher than expected from the other data.

Implications

For the system $(Sr,Ca)CO_3$ it was stated for over 40 years that a phase transition ordered Sr-Cal I↔disordered Sr-Cal II (rotational disorder of CO_3-groups) exists at elevated temperature and pressure (Carlson 1980), which would have an important effect on the composition of coexisting

320 calcite–aragonite. Considering the data presented here (and confirming other recent studies on the
321 $CaCO_3$ endmembers) such a phase transition does not exist. The stability field of Cal-type solid-
322 solutions is shifted towards higher pressures compared to previous assumptions; e.g. the phase
323 transition $R\bar{3}c$ to *Pmcn* of $(Ca_{0.8}Sr_{0.2})CO_3$ at 600°C is expected to occur at 4 kbar rather than
324 1 kbar. Therefore, calcite potentially has a higher relevance for the global Sr cycle than
325 previously assumed; e.g. at 3 kbar the Cal-type solid-solution can incorporate up to 22 mol%
326 contrary to previous assumptions of only 12 mol%.

327 *P-T-X* solid-fluid phase relations and the accurate determination of their composition at variable
328 *P-T* conditions are required for modelling geochemical cycles, especially for modelling the fluid
329 flow, e.g. of the slab component in subduction zones, or during hydrothermal alteration in
330 subvolcanic environments such as porphyries, or during sea-floor metamorphism. Although data
331 on Sr/Ca-distribution between solid and fluid is known for a number of volumetrically important
332 minerals (Dörsam et al. 2007, Liebscher et al. 2009, 2010), these data are limited in the range of
333 *P-T* conditions. In addition, several important mineral groups such as the Ca-zeolites, epidote
334 minerals, and apatite are still missing, and modelling sound scenarios on Sr/Ca distribution e.g.
335 during slab subduction is still premature.

336 For all Ca-rich rocks such as metabasites and metamorphosed marly rocks, f_{CO2} of an externally
337 dominated hydrous fluid controls the presence of carbonates, and thus influences the Sr
338 distribution between solid and fluid. In the presence of an essentially CO_2-free fluid, the fluid is
339 the dominant host for Sr, as the K_d for Sr for Ca-silicates/fluid is always <1.0 (see references
340 above). With increasing f_{CO2} carbonates become modally increasingly important and can be the
341 important host for Sr. This, however, depends strongly on the total *P* as indicated by our data.
342 With increasing P_{tot}, where the two-phase field between calcite and aragonite becomes smaller

and the K_d eventually drops below 1.0, the fluid in equilibrium with carbonates becomes enriched in Sr.

Carbonate stability in basaltic oceanic crust, where carbonates form an integral part, strongly depends on the *P-T* path during subduction and the metamorphic mineral assemblage (Drewitt et al. 2019). Along cool geotherms, more than half of subducted carbonate may be transported past the volcanic front and into the deeper mantle based on phase equilibrium data (Drewitt et al. 2019) and aragonite will become the dominant carbonate phase (Kiseeva et al. 2013). Hence, at ultra-high *P* with a continuous solid solution $(Sr,Ca)CO_3$, Sr is expected to be accumulated in the fluid and can therefore be—depending on the mechanical properties of the rock and the wetting behavior—highly mobile and presumably concentrated either in segregations (Brunsmann et al. 2000) or expelled along the hydrostatic gradient.

The Rb/Sr is used, especially in isotope determinations, as an indicator for closed or open system conditions. The presence of carbonate may significantly influence Rb/Sr, and although Sr is commonly leached during hypogene alteration, leaching may have a smaller effect for Rb/Sr, when carbonates are formed, especially at low pressure.

Since the retrograde transition from aragonite to calcite is very rapid (e.g. Liu and Yund 1993), it is likely that in all high- to ultrahigh-pressure rocks which have been uplifted at temperatures higher than the transformation temperature aragonite–calcite indications for presence of former aragonite-type solid solutions are erased. As Sr shows a higher preference for aragonite than for calcite, any signal for high Sr contents in aragonite may be erased or become indistinct in retrograde calcite. Modelling the geochemical and metamorphic cycle of Sr exclusively based on measured (retrograde) calcite composition may therefore underestimate the role of Sr.

Acknowledgements

We thank Jörg Nissen (ZELMI at TU Berlin) for support in SEM imaging and Dr. Rhede (GFZ Potsdam) for support with EMPA. Financial support was given by the DFG with grant no. FR 557/18 and SCHI 1473/2-1. Critical reading of the manuscript by the anonymous reviewers and editorial handling is gratefully acknowledged.

References

Antao, S.M., and Hassan, I. (2009). The orthorhombic structure of $CaCO_3$, $SrCO_3$, $PbCO_3$ and $BaCO_3$: Linear structural trends. The Canadian Mineralogist, 47(5), 1245-1255.

Antao, S.M., Hassan, I., Mulder, W.H., Lee, P.L., and Toby, B.H. (2009). In situ study of the R3c→R3m orientational disorder in calcite. Physics and Chemistry of Minerals, 36, 159-169.

Armbrust, G.A., Oyarzún, J., Arias, J. (1977). Rb as a guide to ore in Chilean porphyry copper deposits. Economic Geology, 72, 1086-1100.

Armstrong, J.T. (1995). Citzaf - a package of correction programs for the quantitative electron microbeam X-ray-analysis of thick polished materials, thin-films, and particles. Microbeam Analysis, 4, 177-200.

Bagdassarov, N.S., and Slutskii, A.B. (2003). Phase transformations in calcite from electrical impedance measurements. Phase Transitions, 76, 1015-1028.

Bridgman, P.W. (1939). The high pressure behavior of miscellaneous minerals. American Journal of Science, 237, 7-18.

Brunsmann, A., Franz, G., Erzinger, J., Landwehr, D. (2000). Zoisite- and clinozoisite-segregations in metabasites (Tauern Window, Austria) as evidence for high-pressure fluid-rock interaction. Journal of Metamorphic Geology, 18, 1-21.

Carlson, W.D. (1980). The calcite–aragonite equilibrium: effects of Sr substitution and anion orientational disorder. American Mineralogist, 65, 1252-1262.

Carpenter, S.J., and Lohmann, K.C. (1992). Sr/Mg ratios of modern marine calcite: Empirical indicators of ocean chemistry and precipitation rate. Geochimica et Cosmochimica Acta, 56, 1837-1849.

Chang, L.L., and Brice, W.R. (1972). Subsolidus phase relations in aragonite-type carbonates: II. The systems $CaCO_3$-$SrCO_3$-$PbCO_3$ and $CaCO_3$-$BaCO_3$-$PbCO_3$. American Mineralogist: Journal of Earth and Planetary Materials, 57, 155-168.

Chang, L.L. (1965). Subsolidus phase relations in the systems $BaCO_3$-$SrCO_3$, $SrCO_3$-$CaCO_3$, and $BaCO_3$-$CaCO_3$. The Journal of Geology, 73, 346-368.

Chang, L.L. (1971). Subsolidus Phase Relations in the Aragonite-Type Carbonates: I. The System $CaCO_3$-$SrCO_3$-$BaCO_3$. American Mineralogist: Journal of Earth and Planetary Materials, 56, 1660-1673.

Chopin, C., Beyssac, O., Bernard, S., and Malavieille, J. (2008). Aragonite–grossular intergrowths in eclogite-facies marble, Alpine Corsica. European Journal of Mineralogy, 20, 857-865.

Cohen, L.H., and Klement Jr, W. (1973). Determination of high-temperature transition in calcite to 5 kbar by differential thermal analysis in hydrostatic apparatus. The Journal of Geology, 81, 724-727.

Dorsam, G., Liebscher, A., Wunder, B., Franz, G., and Gottschalk, M. (2007). Crystal chemistry of synthetic $Ca_2Al_3Si_3O_{12}OH$–$Sr_2Al_3Si_3O_{12}OH$ solid-solution series of zoisite and clinozoisite. American Mineralogist, 92, 1133-1147.

Dove, M.T., and Powell, B.M. (1989). Neutron diffraction study of the tricritical orientational order/disorder phase transition in calcite at 1260 K. Physics and Chemistry of Minerals, 16, 503-507.

Drewitt, J.W., Walter, M.J., Zhang, H., McMahon, S.C., Edwards, D., Heinen, B.J., Kleppe, A.K. (2019). The fate of carbonate in oceanic crust subducted into earth's lower mantle. Earth and Planetary Science Letters, 511, 213-222.

Dudnikova, V.B., Urusov, V.S., and Eremin, N.N. (2015). Simulation of the local structure, mixing properties, and stability of $CaxSr_{1-}xCO_3$ solid solutions by the interatomic potential method. Physics of the Solid State, 57, 1108-1113.

Fernández-González, A., Prieto, M., Putnis, A., and López-Andrés, S. (1999). Concentric zoning patterns in crystallizing $(Cd,Ca)CO_3$ solid solutions from aqueous solutions. Mineralogical Magazine, 63, 331-343.

Froese, E., and Winkler, H.G.F. (1966). The system $CaCO_3$-$MgCO_3$at high pressures and 500 degrees C to 700 degrees C. The Canadian Mineralogist, 8, 551-566.

Fubini, B., Di Renzo, F., and Stone, F.S. (1988). Strontianite-aragonite solid solutions SrxCa1− xCO3: Effect of composition on the orthorhombic-brhombohedral phase transition and the conversion to oxide solid solutions $SrxCa_{1-}xO$. Journal of Solid State Chemistry, 77, 281-292.

Goldsmith, J.R., and Newton, R.C. (1969). PTX relations in the system $CaCO_3$-$MgCO_3$, at high temperatures and pressures. American Journal of Science, 160-190.

Gottschalk, M. (1997). Internally consistent thermodynamic data for rock-forming minerals in the system SiO_2-TiO_2-Al_2O_3-Fe_2O_3-CaO-MgO-FeO-K_2O-Na_2O-H_2O-CO_2. European Journal of Mineralogy, 9, 175-223.

Ter Heege, J.H., and Renner, J. (2007). In situ impedance spectroscopy on pyrophyllite and $CaCO_3$ at high pressure and temperature: phase transformations and kinetics of atomistic transport. Physics and Chemistry of Minerals, 34, 445-465.

Holland, H.D., Borcsik, M., Munoz, J., and Oxburgh, U.M. (1963). The coprecipitation of Sr^{+2} with aragonite and of Ca^{+2} with strontianite between 90 and 100 C. Geochimica et Cosmochimica Acta, 27, 957-977.

Jamieson, J.C. (1953). Phase equilibrium in the system calcite-aragonite. The Journal of Chemical Physics, 21, 1385-1390.

Jamieson, J.C. (1957). Introductory studies of high-pressure polymorphism to 24,000 bars by X-ray diffraction with some comments on calcite II. The Journal of Geology, 65, 334-343.

Jarosch, D., and Heger, G. (1988). Neutron diffraction investigation of strontianite, $SrCO_3$. Bulletin de Minéralogie, 111, 139-142.

Jarosewich, E., and MacIntyre, I.G. (1983). Carbonate Reference Samples for Electron Microprobe and Scanning Electron Microscope Analyses: RESEARCH-METHOD PAPER. Journal of Sedimentary Research, 53, 677-678.

Jarosewich, E., and White, J.S. (1987). Strontianite reference sample for electron microprobe and SEM analyses. Journal of Sedimentary Research, 57, 762-763

Katz, A.M.I.T.A.I., Sass, E., Starinsky, A., and Holland, H.D. (1972). Strontium behavior in the aragonite-calcite transformation: An experimental study at 40–98 C. Geochimica et Cosmochimica Acta, 36, 481-496.

Kiseeva, E.S., Litasov, K.D., Yaxley, G.M., Ohtani, E., Kamenetsky, V.S. (2013). Melting and phase relations of carbonated eclogite at 9–21 GPa and the petrogenesis of alkali-rich melts in the deep mantle. Journal of Petrology, 54, 1555-1583.

Kondo, S., Suito, K., and Matsushima, S. (1972). Ultrasonic observation of calcite I-II inversion to 700 C. Journal of Physics of the Earth, 20, 245-250.

Kump, L.R. (1989). Alternative modeling approaches to the geochemical cycles of carbon, sulfur, and strontium isotopes. American Journal of Science, 289, 390-410.

Larson, A.C., and Von Dreele, R.B. (1994). Generalized structure analysis system (GSAS). Los Alamos National Laborator Report LAUR, 86-748.

Liebscher, A., Thiele, M., Franz, G., Dörs m, G., and Gottschalk, M. (2009). Synthetic Sr–Ca margarite, anorthite and slawsonite solid solutions and solid–fluid Sr–Ca fractionation. European Journal of Mineralogy, 21, 275-292.

Liebscher, A., Dörsam, G., Franz, G., Wunder, B., and Gottschalk, M. (2010). Crystal chemistry of synthetic lawsonite solid-solution series $CaAl_2[(OH)_2/Si_2O_7]\cdot H_2O$ – $SrAl_2[(OH)_2/Si_2O_7]\cdot H_2O$ and the Cmcm–P21/m phase transition. American Mineralogist, 95, 724-735.

Liu, L.-G. and Bassett, W.A. (1986). Elements, oxides, and silicates: high-pressure phases with implications for the earth's interior. Oxford University Press, New York

Liu, M., and Yund, R.A. (1993). Transformation kinetics of polycristalline aragonite to calcite: new experimental data, modelling, and implications. Contributions Mineralogy and Petrology, 114, 465-478.

Lucas-Girot, A., Hernandez, O., and Oudadesse, H. (2007). Re-examination of the structural properties of solid solutions $SrxCa_{1-}xCO_3$. Materials research bulletin, 42, 1061-1068.

Manning, C.E. (2014). Geochemistry: A piece of the deep carbon puzzle. Nature Geoscience, 7, 333.

Markgraf, S.A., and Reeder, R.J. (1985). High-temperature structure refinements of calcite and magnesite. American Mineralogist, 70, 590-600.

Mirwald, P.W. (1976). A differential thermal analysis study of the high-temperature polymorphism of calcite at high pressure. Contributions to Mineralogy and Petrology, 59, 33-40.

Mirwald, P.W. (1979). The electrical conductivity of calcite between 300 and 1200 C at a CO 2 pressure of 40 bars. Physics and Chemistry of Minerals, 4, 291-297.

Putnis, A. (2002). Mineral replacement reactions: from macroscopic observations to microscopic mechanisms. Mineralogical Magazine, 66, 689-708.

Putnis, A., and Putnis, C.V. (2007). The mechanism of reequilibration of solids in the presence of a fluid phase. Journal of Solid State Chemistry, 180, 1783-1786.

Putnis, A. (2009). Mineral replacement reactions. Reviews in mineralogy and geochemistry, 70, 87-124.

Redfern, S.A.T., Salje, E., and Navrotsky, A. (1989). High-temperature enthalpy at the orientational order-disorder transition in calcite: implications for the calcite/aragonite phase equilibrium. Contributions to Mineralogy and Petrology, 101, 479-484.

Shannon, R.D. (1976). Revised effective ionic radii and systematic studies of interatomic distances in halides and chalcogenides. Acta crystallographica section A: crystal physics, diffraction, theoretical and general crystallography, 32, 751-767.

Speer, J.A. (1983). Crystal chemistry and phase relations of orthorhombic carbonates. Reviews in Mineralogy and Geochemistry, 11, 145-190.

Vegard, L., and Dale, H. (1928). VIII. Untersuchungen über Mischkristalle und Legierungen. Zeitschrift für Kristallographie-Crystalline Materials, 67, 148-162.

Wang, L., Sondi, I., and Matijević, E. (1999). Preparation of uniform needle-like aragonite particles by homogeneous precipitation. Journal of Colloid and Interface Science, 218, 545-553.

Figure captions

Figure 1. (A) Isobaric (2 kbar) T-x_{SrCO3} relations and (B) isothermal (T = 600°C) P-x_{SrCO3} relations for $CaCO_3$-$SrCO_3$ with a two-phase field between orthorhombic and trigonal carbonate phases and the postulated transition of ordered-disordered $CaCO_3$ (modified from Carlson 1980) at 8 kbar/600°C. (C) Calcite I-aragonite stability (Liou and Basset 1986; solid line) and metastable transitions to calcite II, II, IV, and V (Bagdassarov and Slutskii 2003; Bridgman1939; Kondo et al. 1972; dashed lines). Thin dashed line indicates the postulated transition between

512 ordered and disordered calcite I (Goldsmith and Newton 1969), 600°C at 8 kbar which was
513 rejected later but used by Carlson (1980) for constructing stability fields in the system
514 (Sr,Ca)CO_3 (red circles).

515

516 **Figure 2.** Mineral phase content and of run products of type I (Cal+Str), type II (Cal+Arg), and
517 type III (Sr-Arg) syntheses based on XRD analyses.

518

519 **Figure 3.** Lattice constants of orthorhombic and trigonal $CaCO_3$-$SrCO_3$ synthesized in this study
520 and compared to literature data (Antao and Hassan 2009; Fubini et al. 1988; Holland et al. 1963;
521 Lucas-Girot et al. 2007;). For the orthorhombic carbonates a linear correlation is well established.
522 The extrapolated lattice constants for trigonal $SrCO_3$ are a = 5.08±0.02 Å and c = 17.62±0.10 Å.
523 Errors are estimated based on the extrapolation of maximum and minimum slopes within the
524 upper and lower confidence levels towards the Sr-endmember using a 95% confidence band
525 (shaded grey area).

526

527 **Figure 4.** SE and EMPA BSE images of selected runs for all types of syntheses. Pressure and
528 temperature are denoted in the upper part of each image. Str and Cal refers to strontianite and
529 calcite, respectively. The subscripts "ss" denotes a solid solute

530

531 **Figure 5.** Calculated P-X_{SrCO3}-relations (isothermal T = 600°C) with a two-phase field between
532 calcite- and aragonit-type solid solutions, based on experimental results from this study. For the

orthorhombic limb, the data agree well with the data determined by Carlson (1980), for the trigonal limb these data underestimate the amount of $SrCO_3$ in calcite, except at atmospheric pressure (Chang 1965). In addition, there is no evidence for a transition between ordered and disordered calcite.

Figure 6. (A) Measured concentration of Sr and Ca in the fluid after run (expressed as molar X_{Sr}^{fluid}) versus $X_{Sr}^{carbonate}$ in trigonal and orthorhombic carbonate. Average K_d for Cal-type carbonate is near 1.0, for Arg-type carbonate it varies from 1.7 to 3.1. (B) For Cal_{ss} and Arg_{ss} there is a tendency of decreasing K_d-values with increasing pressure. A Linear trend is plotted for visualization (grey datapoints are excluded–see text).

This is the peer-reviewed, final accepted version for American Mineralogist, published by the Mineralogical Society of America.
The published version is subject to change. Cite as Authors (Year) Title. American Mineralogist, in press.
DOI: https://doi.org/10.2138/am-2021-7783. http://www.minsocam.org/

Tables

Table 1. Starting materials (Cal: calcite, Str: strontianite, Arg: aragonite, Sr-Arg: Sr-rich aragonite), initial weights, and experimental conditions of all autoclave runs.

	Run no.	Capsule material	P (kbar)	T (°C)	Components in starting mixture	X_{Sr} (bulk initial)	Mass of solids (mg)	H_2O (mg)	Time (d)
Type I	P1	Au	2	600	Cal+Str	0.446	53.01	11.97	3
	P2	Au	3	600	Cal+Str	0.323	45.80	10.02	3
	P3	Au	1	600	Cal+Str	0.323	53.14	9.51	3
	P5	Au	1	600	Cal+Str	0.350	80.94	9.87	7
	P6[a]	Au	1	550	Cal+Str	0.247	59.97	8.84	7
	P7	Au	1	600	Cal+Str	0.247	69.59	9.44	22
	P8[a]	Au	1	600	Cal+Str	0.239	69.33	9.88	22
	P11	Pt	1	600	Cal+Str+AgOx[b]	0.250	143.80	20.52	14
	P12	Pt	2	600	Cal+Str+AgOx[b]	0.250	130.24	20.38	14
Type II	P9	Pt	2	600	Arg+Str	0.252	71.32	19.40	14
	P10	Pt	1	600	Arg+Str	0.266	140.07	19.00	14
	P13	Pt	0.5	600	Arg+Str	0.400	135.45	20.00	14
	P14	Pt	3	600	Arg+Str	0.300	124.1	18.24	14
	P15	Pt	4	600	Arg+Str	0.250	143.07	20.90	14
	P16	Pt	5	600	Arg+Str	0.250	154.55	20.10	14
Type III	P17	Au	2	600	Sr-Arg	0.24	141.84	19.97	14
	P18	Au	3	600	Sr-Arg	0.24	99.53	19.09	14
	P19	Au	4	600	Sr-Arg	0.24	101.24	20.76	14
	P20	Au	5	600	Sr-Arg	0.24	99.43	17.77	14
	P21	Au	0.5	600	Sr-Arg	0.37	86.28	20.27	14
	P22	Au	1	600	Sr-Arg	0.37	94.74	20.36	14

[a] rapid quench system at the GFZ Potsdam; [b]AgOx: 10.74 mg (P11) and 9.89 mg (P12) of silveroxalate;

This is the peer-reviewed, final accepted version for American Mineralogist, published by the Mineralogical Society of America.
The published version is subject to change. Cite as Authors (Year) Title. American Mineralogist, in press.
DOI: https://doi.org/10.2138/am-2021-7783. http://www.minsocam.org/

547

548 **Table 2.** EMPA analyses of all runs arranged by type of experiment and increasing pressure. Standard
549 deviation (2σ) is given for the purpose of identifying runs with highly heterogeneous phase compositions
550 which includes measuring compositional zoning. Data is not normally distributed; n = number of spot
551 analyses.

Run no.	Pressure (kbar)	Components in starting mixture	Initial bulk x_{Sr}	Composition orthorhombic phase (mol% $SrCO_3$)		Composition trigonal phase (mol% $SrCO_3$)	
				mean ± 2σ	n	mean ± 2σ	n
P3	1	Cal+Str	32.3	68.0 ± 33.7	12	- ± -	-
P5	1	Cal+Str	35.0	-	-	-	-
P6[a]	1	Cal+Str	24.7	71.0 ± 31.5	12	0.1 ± 0.0	3
P7	1	Cal+Str	24.7	58.7 ± 11.1	11	0.1 ± 0.1	3
P8[a]	1	Cal+Str	23.9	74.1 ± 41.5	9	0.1 ± 0.0	2
P11	1	Cal+Str+ AgOx[b]	25.0	62.2 ± 35.3	6	0.1 ± 0.0	4
P1	2	Cal+Str	44.6	60.4 ± 34.3	16	- ± -	-
P12	2	Cal+Str+ AgOx[b]	25.0	52.6 ± 12.8	15	0.1 ± 0.1	4
P2	3	Cal+Str	32.3	69.6 ± 45.9	11	0.1 ± 0.3	2
P13	0.5	Arg+Str	40.0	56.7 ± 4.5	13	25.9 ± 2.6	10
P10	1	Arg+Str	26.6	53.8 ± 0.9	6	15.3 ± 19.4	8
P9	2	Arg+Str	25.2	51.8 ± 1.2	3	8.5 ± 18.9	5
P14	3	Arg+Str	30.0	40.2 ± 5.6	13	1.3 ± 0.7	11
P15	4	Arg+Str	25.0	53.3 ± 15.6	14	1.2 ± 0.6	14
P16	5	Arg+Str	25.0	43.5 ± 2.6	12	2.4 ± 7.1	15
P21	0.5	Sr-Arg	37.0	54.2 ± 2.0	12	26.0 ± 1.0	12
P22	1	Sr-Arg	37.0	53.1 ± 1.7	14	23.7 ± 7.4	13
P17	2	Sr-Arg	24.0	49.4 ± 1.3	12	21.2 ± 11.9	14
P18	3	Sr-Arg	24.0	44.6 ± 3.8	16	18.5 ± 13.3	15
P19	4	Sr-Arg	24.0	41.8 ± 2.7	13	18.8 ± 11.2	15
P20	5	Sr-Arg	24.0	38.8 ± 2.8	11	14.8 ± 12.5	13

[a] rapid quench system at the GFZ Potsdam; [b]AgOx: 10.74 mg (P11) and 9.89 mg (P12) of silveroxalate

552 **Table 3.** Composition of Arg-type and Cal-type solid solutions from selected runs, for which near-
553 equilibrium compositions are assumed, based on EMPA (error = 2σ; n = number of EMPA spot analyses)
554 and powder XRD, X_{Sr} of coexisting fluid (error = 5%), and K_d-values of Arg-type and Cal-type solid
555 solution (error propagation of relative errors).

run no.	**P21**	**P13**	**P22**	**P10**	**P17**	**P9**	**P18**	**P19**	**P20**
P (kbar)	0.5	0.5	1	1	2	2	3	4	5
X_{Sr}^{fluid}	0.215±0.011	-	0.237±0.012	0.203±0.010	0.175±0.008	0.165±0.012	0.240±0.012	0.237±0.012	0.229±0.011
					Arg_{ss}				
$SrCO_3$ mean (mol%)	54.2±2.0	56.7±4.5	53.1±1.7	53.8±0.9	49.4±1.3	51.8±1.2	44.6±3.8	41.8±2.7	38.8±2.8
n	12	13	14	6	12	3	16	13	11
K_d	2.5±0.2	-	2.2±0.2	2.7±0.2	2.8±0.2	3.1±0.2	1.9±0.3	1.8±0.2	1.7±0.2
					Cal_{ss}				
$SrCO_3$ mean (mol%)	26.0±1.0	25.9±2.6	24.7±1.2	22.5±1.3	24.6±2.6	18.7±6.6	22.3±2.2	21.4±2.5	18.4±0.5
n	12	10	12	4	10	2	11	12	9
K_d	1.2±0.1	-	1.0±0.1	1.1±0.1	1.4±0.2	1.1±0.5	0.9±0.1	0.9±0.2	0.8±0.1

556

557

This is the peer-reviewed, final accepted version for American Mineralogist, published by the Mineralogical Society of America.
The published version is subject to change. Cite as Authors (Year) Title. American Mineralogist, in press.
DOI: https://doi.org/10.2138/am-2021-7783. http://www.minsocam.org/

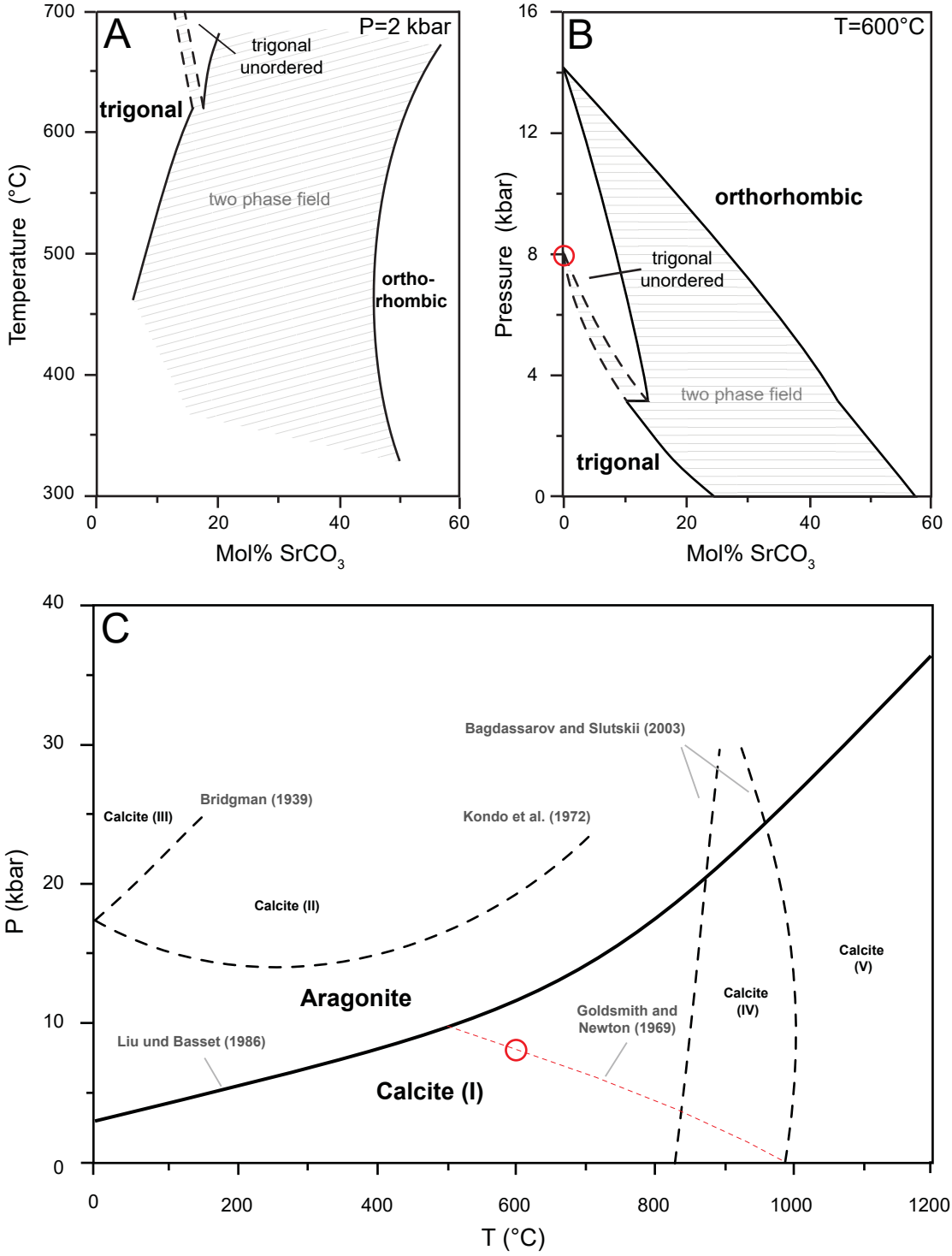

This is the peer-reviewed, final accepted version for American Mineralogist, published by the Mineralogical Society of America.
The published version is subject to change. Cite as Authors (Year) Title. American Mineralogist, in press.
DOI: https://doi.org/10.2138/am-2021-7783. http://www.minsocam.org/

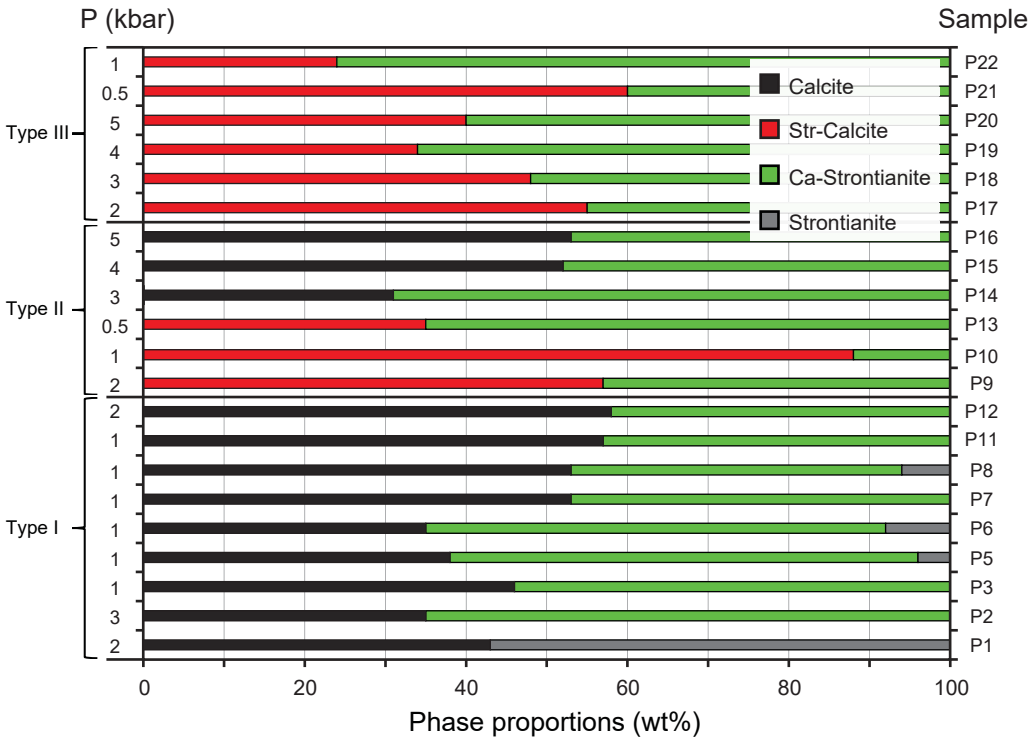

This is the peer-reviewed, final accepted version for American Mineralogist, published by the Mineralogical Society of America.
The published version is subject to change. Cite as Authors (Year) Title. American Mineralogist, in press.
DOI: https://doi.org/10.2138/am-2021-7783. http://www.minsocam.org/

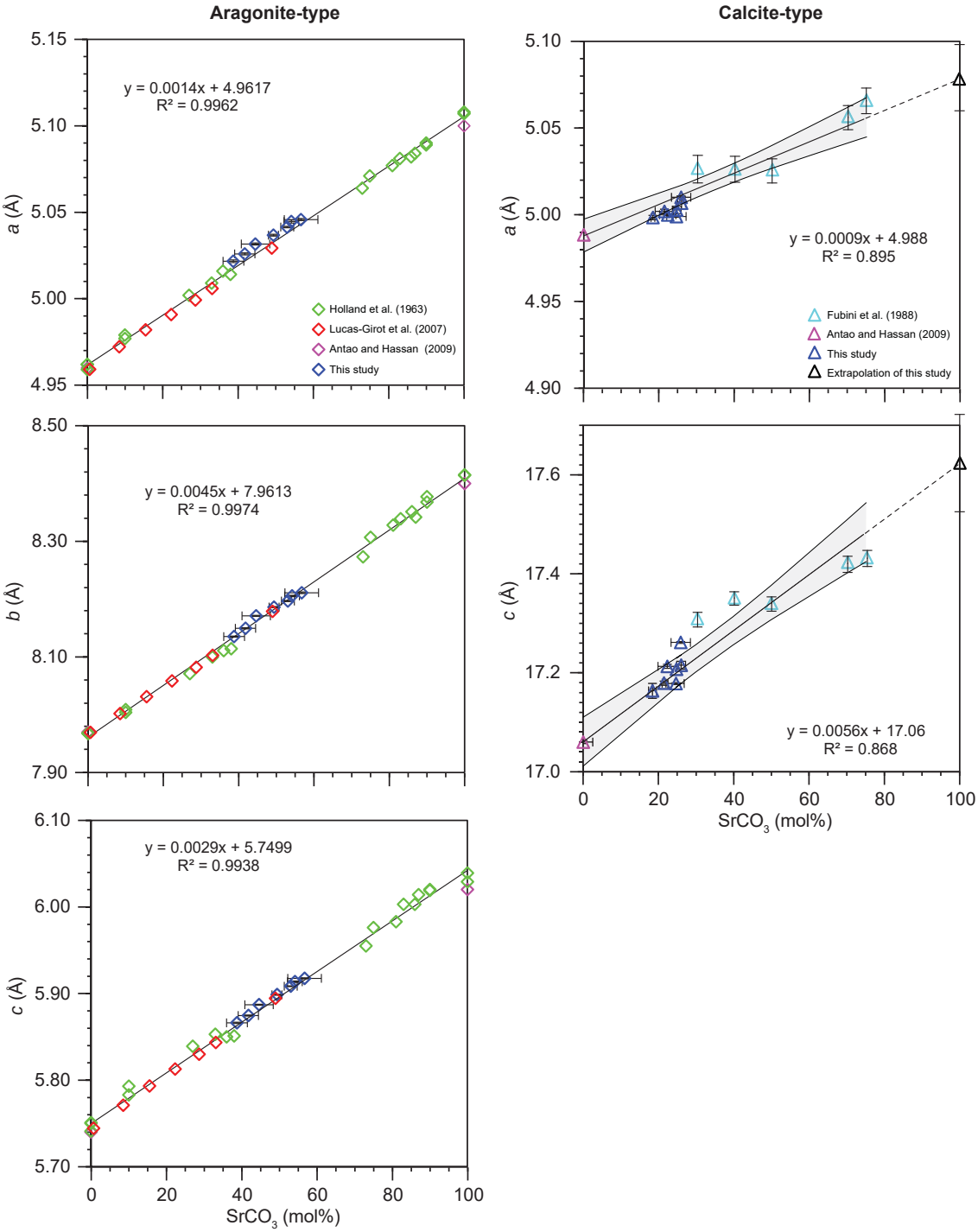

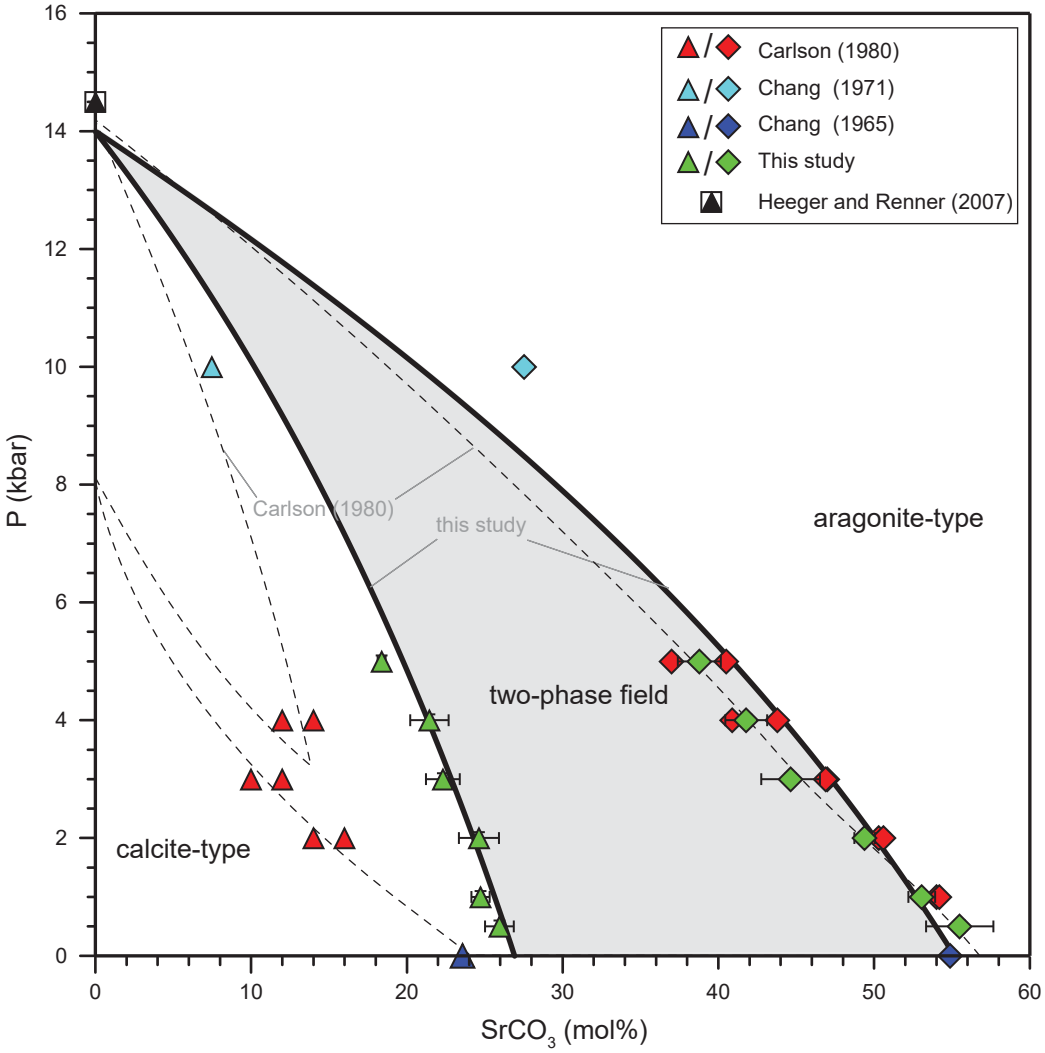

This is the peer-reviewed, final accepted version for American Mineralogist, published by the Mineralogical Society of America.
The published version is subject to change. Cite as Authors (Year) Title. American Mineralogist, in press.
DOI: https://doi.org/10.2138/am-2021-7783. http://www.minsocam.org/

Figure 6

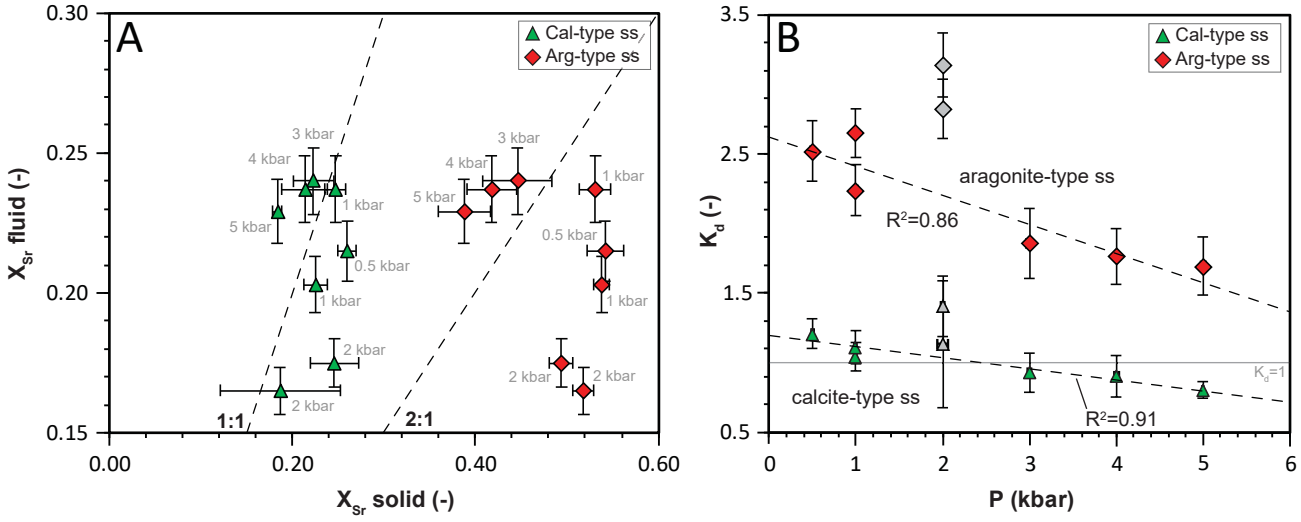

Figure 4